

Resorcinol Derivative as an Environmentally Friendly Low Carbon Steel Inhibitor in HCl Medium

Medhat M. Kamel, Salah M. Rashwan, Mostafa A. A. Mahmoud,* Sameh A. A. El-Mekawy, Mohamed K. Awad, and Hoyeda E. Ibrahim



Cite This: *ACS Omega* 2022, 7, 17609–17619



Read Online

ACCESS |



Metrics & More

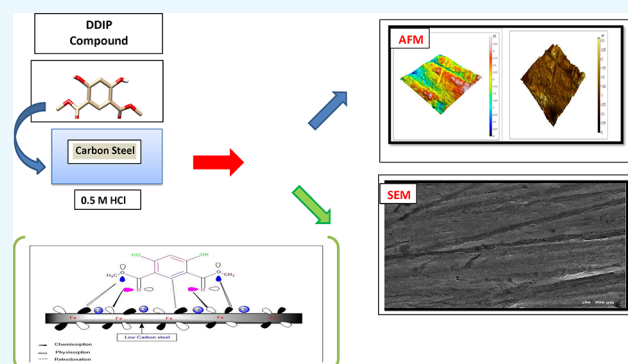


Article Recommendations



Supporting Information

ABSTRACT: An ecofriendly resorcinol derivative, dimethyl-4,6-dihydroxisophthalate (DDIP) is examined as an anticorrosion agent for low carbon steel (CS) in a 0.5 mol L⁻¹ HCl solution. Electrochemical and chemical methods are used to determine the effectiveness of the inhibitor. The DDIP compound decreased the rate of CS corrosion. The mitigation efficiency rose from 61.8 to 79.9% as the DDIP dose increased from 50 to 300 ppm in the corrosive medium. At 300 ppm, however, the efficiency decreased from 79.9 to 70.05% as the temperature increased from 25 to 55 °C. Physical quantities and thermodynamic parameters are discussed. The compound's adsorption follows Langmuir's concept. Adsorption of the DDIP compound is a mix of physisorption and chemisorption. The difference in E_{corr} values is less than 85 mV, indicating that the examined compound is a mixed-type inhibitor. Scanning electron microscopy and atomic force microscopy revealed the development of a coherent film at CS in the presence of the DDIP inhibitor. The results obtained using various techniques were closely related, indicating validity and accuracy. The interaction between the DDIP molecules and the CS was explained by the density functional theory and Monte Carlo simulation. The quantum characteristics confirmed that the DDIP compound is a promising inhibitor.



1. INTRODUCTION

Carbon steel (CS) is widely used for drilling and transportation pipelines in the oil and gas industry. The bulk of acidic industrial applications relies on carbon steel, such as pickling, industrial cleaning, and crude oil refining, descaling, and petrochemical processes. CS alloys are also inexpensive and have properties superior to those of other metal alloys. HCl is commonly used in the industrial sector for cleaning and descaling procedures. The fundamental problem with this procedure is that when carbon steel is exposed to an acidic environment, it rusts.^{1–5} In addition, the acid is also produced during the cracking of petroleum as a result of salt hydrolysis.⁶

Corrosion occurs when clean Fe metal reverts to its original state, Fe₂O₃, due to electrochemical reactions with nearby media such as H₂S, CO₂, and H₂O. Corrosion impacts all metallic infrastructure in the oil field such as pipes, tanks, and separators at all stages of production. Pipes, tanks, and plumbing systems develop cracks or pits.^{7,8} In terms of corrosion, hydrochloric acid is by far the most commonly used acid.⁹

The use of adsorption inhibitors in acidic conditions is a standout among many other ideals and material ways of managing steel corrosion.¹⁰ Because of its importance in applications, the corrosion behavior of CS in acid environ-

ments is of great importance. The most efficient procedure for protecting metals from corrosion is using chemical compounds as corrosion inhibitors. These compounds reduce the corrosion rate.^{11–18} The substance that is considered to be eco-friendly and safe for humans when prepared is the best choice for use as a corrosion inhibitor. Many investigations about the utilization of drugs as potential candidates for metal corrosion mitigation have recently been conducted. Their structures permit the formation of complexes with metallic ions on the metal surfaces.^{19–23}

Resorcinol, a safe compound, is used as an antiseptic and disinfectant in pharmaceutical drugs. Furthermore, it is inexpensive, widely available, nontoxic, and environmentally benign. Because of these characteristics, resorcinol derivatives were selected for corrosion studies.

The primary goal of this research is to examine the inhibition performance of the DDIP compound for CS

Received: January 8, 2022

Accepted: April 11, 2022

Published: May 16, 2022



demonstrates the results of CS tests in 0.5 mol L⁻¹ HCl acid with and without distinct amounts of the DDIP compound. The inhibition efficacy of the compound increases as its amount in the corrosive solution increases.

3.2. Impact of Temperature on Inhibition Efficacy.

The influence of solution temperature on the inhibition efficacy is determined at 25, 35, 45, and 55 °C, and the findings are shown in Tables 2 and 3. The effectiveness of inhibition

Table 2. Carbon Steel Corrosion Rate after Immersion in 0.5 mol L⁻¹ HCl with and without Different Concentrations of the DDIP Compound at Different Temperatures

concn (ppm)	DDIP			
	CR (kg·m ⁻² ·s ⁻¹ × 10 ⁻⁹) at 240 min			
	25 °C	35 °C	45 °C	55 °C
blank	78.00 ± 0.2	80.00 ± 0.3	83.00 ± 0.5	86.00 ± 0.2
50	30.07 ± 0.3	33.75 ± 0.2	37.08 ± 0.3	43.75 ± 0.4
100	27.5 ± 0.5	30.42 ± 0.4	35.42 ± 0.1	39.58 ± 0.1
150	24.25 ± 0.2	27.08 ± 0.5	32.08 ± 0.4	36.67 ± 0.3
200	20.43 ± 0.1	25.42 ± 0.4	29.17 ± 0.3	33.75 ± 0.2
250	18.82 ± 0.3	20.83 ± 0.1	27.08 ± 0.1	32.5 ± 0.5
300	15.86 ± 0.4	20.00 ± 0.2	21.67 ± 0.2	25.83 ± 0.6

decreases as the temperature increases. The decrease in inhibition efficacy is ascribed to the detachment of the compound molecules from the steel surface as the temperatures increases.

3.3. Thermodynamic Activation Parameters of the Corrosion Reaction. Thermodynamic parameters are a crucial and significant tool to understand inhibitor adsorption behavior. The activation energy (E_a^*), enthalpy change (ΔH_a^*), and entropy change (ΔS_a^*) of activation for the dissolution of CS in 0.5 mol L⁻¹ HCl solution were estimated. Arrhenius and transition-state equations were used to calculate the parameters in the absence and presence of the DDIP chemical compound.

$$k = A \exp\left(\frac{-E_a^*}{RT}\right) \quad (3)$$

$$\ln\left(\frac{k}{T}\right) = \ln\left(\frac{k_B}{h}\right) + \left(\frac{\Delta S_a^*}{R}\right) - \frac{\Delta H_a^*}{RT} \quad (4)$$

where k is the dissolution rate, R is the gas constant, k_B is the Boltzmann constant, T is the Kelvin temperature, and h indicates Planck's constant. The Arrhenius plot ($\log k$ vs $1/T$) and transition-state plots ($\log k/T$ vs $1/T$) of the DDIP compound are shown in Figure 1.

The Arrhenius plot shows a straight line with a slope of $-E_a^*/2.303R$, through which the E_a value of the impeded dissolution process of CS is evaluated and listed in Table 4. The E_a^* has a value of 3.5 kJ mol⁻¹ for the blank solution. Because the DDIP compound inhibits the corrosion process, the activation energy significantly increases with varying concentrations of the organic compound. This variation might be ascribed either to the precipitation of the DDIP compound at the CS surface or a variation in the potential difference of the metal solution boundary caused by adsorption. Transition-state plots exhibit straight lines with slopes of $-(\Delta H_a^*)/(2.303R)$ and intercept $\log(k_B/h) + \Delta S_a^*/R$, by which ΔS_a^* and ΔH_a^* quantities were evaluated (Table 4). The positivity of ΔH_a^* reveals that the formation of the activated complex is an endothermic process. The negativity of ΔS_a^* suggests that the molecules of DDIP were adsorbed in an organized way over the CS surface.²⁶

3.4. Adsorption Considerations. The adsorption isotherm is required to understand the adsorption mechanism. The experimental data were examined using many adsorption isotherms such as Langmuir, Freundlich, Temkin, and Flory–Huggins to learn more about the DDIP's adsorption at CS. For the Langmuir model, the best fit is recognized with a regression coefficient of $R^2 = 0.9994$, confirming the feasibility of this approach.²⁷ The Langmuir adsorption isotherm presumes that all adsorption centers are equivalent and possess similar energy characteristics.²⁸ The preceding formula is used to compute the Langmuir isotherm.

$$\frac{C}{\theta} = \frac{1}{K_{\text{ads}}} + C \quad (5)$$

K_{ads} denotes the equilibrium constant for adsorption. The Langmuir isotherm of the compound DDIP at the CS surface is shown in Figure 2. Table 5 comprises data gathered from this isotherm. The departure of the slopes from unity is ascribed to interactions of the adsorbed organic species, a component that is not considered throughout the development of the Langmuir equation. The following equation is used to compute the standard free energy change of the adsorption ($\Delta G_{\text{ads}}^\circ$).²⁹

Table 3. Data of Weight Loss Measurements at 240 min for CS in 0.5 mol L⁻¹ HCl in the Absence and Presence of Different Concentrations of DDIP Compound at Different Temperatures

concn (ppm)	DDIP										
	25 °C			35 °C			45 °C			55 °C	
	θ	%IE	concn (ppm)	θ	%IE	concn (ppm)	θ	%IE	concn (ppm)	θ	%IE
0			0			0			0		
50	0.618	61.8 ± 0.2	50	0.574	57.37 ± 0.3	50	0.544	54.36 ± 0.3	50	0.493	49.28 ± 0.3
100	0.649	65.1 ± 0.1	100	0.616	61.58 ± 0.2	100	0.564	56.41 ± 0.1	100	0.541	54.11 ± 0.2
150	0.692	69.2 ± 0.3	150	0.658	65.79 ± 0.3	150	0.605	60.51 ± 0.3	150	0.575	57.49 ± 0.4
200	0.740	74.0 ± 0.5	200	0.679	67.89 ± 0.4	200	0.641	64.1 ± 0.4	200	0.609	60.87 ± 0.1
250	0.760	76.0 ± 0.4	250	0.737	73.68 ± 0.2	250	0.667	66.67 ± 0.2	250	0.623	62.32 ± 0.5
300	0.799	79.9 ± 0.3	300	0.747	74.74 ± 0.4	300	0.733	73.33 ± 0.2	300	0.700	70.05 ± 0.2

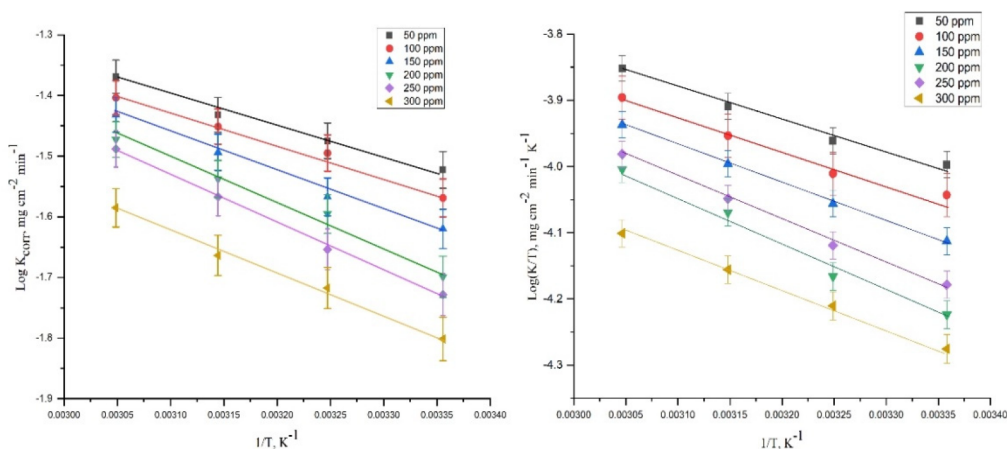


Figure 1. Arrhenius plots ($\log k$ vs $1/T$) and transition-state plots ($\log k/T$ vs $1/T$) for corrosion of carbon steel in 0.5 mol L^{-1} HCl without and with different concentrations of the compound DDIP.

Table 4. Activation Parameters for the Dissolution of CS in the Absence and Presence of Different Doses of the Compound DDIP in 0.5 mol L^{-1} HCl

concn (ppm)	E_a^* (kJ mol^{-1})	R^2	ΔH^* (kJ mol^{-1})	$-\Delta S^*$ ($\text{J mol}^{-1} \text{K}^{-1}$)
blank	3.5	0.94	0.9	263
50	5.1	0.92	2.5	268
100	6.5	0.95	4.2	263
150	8.0	0.95	5.4	61
200	8.4	0.94	5.8	60
250	9.6	0.94	7.1	57
300	10.1	0.95	7.5	56

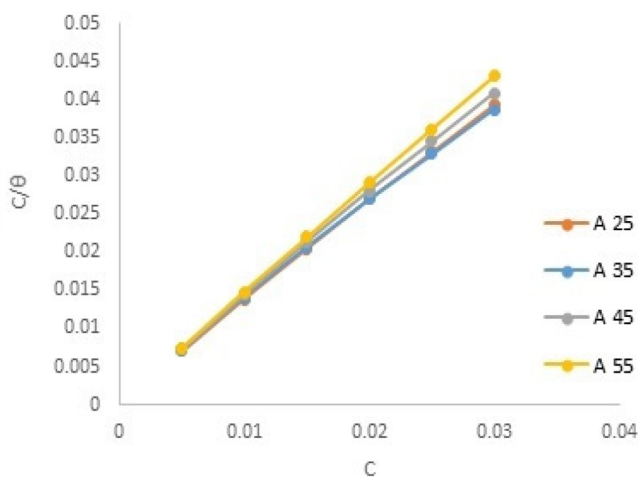


Figure 2. Langmuir adsorption isotherms for CS in 0.5 mol L^{-1} HCl in the presence of the DDIP compound at different temperatures.

$$K_{\text{ads}} = \frac{1}{55.5} \exp\left(\frac{-\Delta G^{\circ}}{RT}\right) \quad (6)$$

where 55.5 is the molar quantity of H_2O . The fact that $\Delta G^{\circ}_{\text{ads}}$ values are negative confirms the durability of the adsorbed film at the CS surface.³⁰ It has been reported that $\Delta G^{\circ}_{\text{ads}}$ values up to -20 kJ mol^{-1} are preserved for electrostatic attraction between charged molecules and charged metals. However, those greater than -40 kJ mol^{-1} implicate electron transfer from the inhibitor to the metal surface to form a coordinating bond.³¹ The $\Delta G^{\circ}_{\text{ads}}$ reported in this study ranged between

Table 5. Equilibrium Constant K_{ads} and Standard Free Energy $\Delta G^{\circ}_{\text{ads}}$ of Adsorption of the DDIP Compound on CS in 0.5 mol L^{-1} HCl at Different Temperatures

temp ($^{\circ}\text{C}$)	DDIP				
	slope	intercept $\times 10^{-5}$	$K_{\text{ads}} \times 10^{-3}$ (mol^{-1})	$-\Delta G^{\circ}$ (kJ mol^{-1})	R^2
25	1.29	91.5	1092.8	27.3	0.9995
35	1.26	137.6	726.6	25.8	0.9995
45	1.34	96.8	1033.5	26.7	0.9995
55	1.43	48.9	2084.1	28.4	0.9999

-25.8 and $-28.4 \text{ kJ mol}^{-1}$. This verifies that the DDIP inhibitor reduces the rate of corrosion of CS via physisorption and chemisorption processes. A good agreement with the Langmuir isotherm, according to Latour, does not imply that the model is acceptable for the adsorption process. Perhaps the value obtained for K_{eq} could be regarded as a semiquantitative descriptor of the isotherm shape.³²

3.5. PP Measurements. Figure 3 depicts the Tafel plots of CS in 0.5 mol L^{-1} HCl in the presence and absence of varying

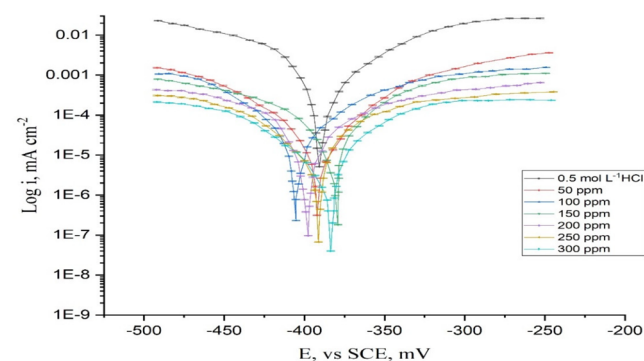


Figure 3. Plots of potentiodynamic polarization measurements for dissolution of CS without and with different concentrations of compound DDIP at $25 \text{ }^{\circ}\text{C}$.

dosages of the DDIP organic compound at $25 \text{ }^{\circ}\text{C}$. Table 6 shows the derived kinetic factors such as corrosion current (I_{corr}), Tafel slopes (β_c and β_a), corrosion potential (E_{corr}), and inhibition efficacy (IE). In the presence of the DDIP compound, I_{corr} decreases; however, %IE increases. Also, β_a and β_c were unaffected. The Tafel lines ran parallel, indicating

Table 6. Potentiodynamic Polarization Parameters of CS in 0.5 mol L⁻¹ HCl Containing Different Concentrations of the Compound DDIP at 25 °C

concn (ppm)	DDIP						%IE
	$-E_{\text{corr}}$ (V vs SCE) $\times 10^{-3}$	β_a (V dec ⁻¹) $\times 10^{-3}$	β_c (-V dec ⁻¹) $\times 10^{-3}$	I_{corr} (A/cm ²) $\times 10^{-3}$	θ		
blank	391	242	322	1.52			
50	393	228	288	0.60	0.605	60.5 \pm 0.2	
100	406	207	250	0.53	0.651	65.1 \pm 0.1	
150	380	190	248	0.49	0.677	67.7 \pm 0.3	
200	398	189	220	0.41	0.730	73.0 \pm 0.4	
250	390	182	190	0.35	0.769	76.9 \pm 0.5	
300	384	118	150	0.27	0.822	82.2 \pm 0.1	

that the inhibitory action of the DDIP compound is caused by simply blocking the accessible surface area by adsorption; that is, the examined compound reduces metal disintegration and hydrogen evolution while not affecting the reaction mechanism.³³ The difference in E_{corr} values does not attain 85 mV, indicating that the examined compound is a mixed-type inhibitor.

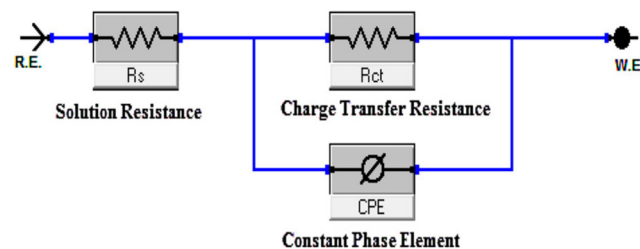
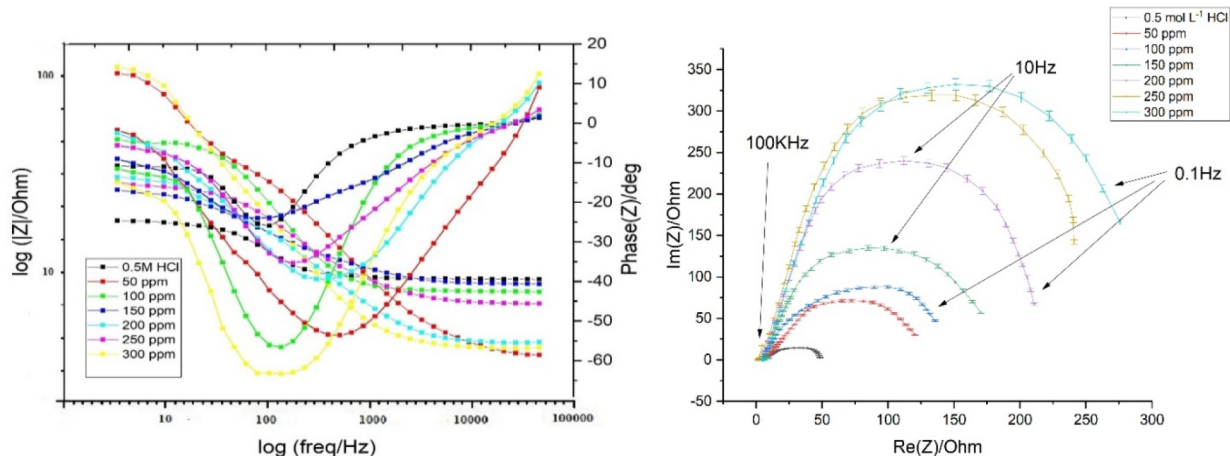
3.6. EIS Measurements. Table 7 summarizes the data derived from EIS measurements for the dissolution of CS in

Table 7. EIS Data of CS in 0.5 mol L⁻¹ HCl in the Absence and Presence of Different Concentrations of the DDIP Compound at 25 °C

concn (ppm)	DDIP			
	R_{ct} (Ω cm ²)	C_{dl} (F cm ⁻²) $\times 10^{-6}$	θ	%IE
blank	48.6	108		
50	120.3	45	0.596	59.6 \pm 0.3
100	135.7	38	0.642	64.2 \pm 0.1
150	170.4	26	0.715	71.5 \pm 0.4
200	210.6	22	0.769	76.9 \pm 0.2
250	241.0	17	0.798	79.8 \pm 0.1
300	275.7	15	0.824	82.4 \pm 0.4

the presence of the DDIP compound and 0.5 mol L⁻¹ HCl at room temperature. Figure 4 depicts the Nyquist (right) and Bode (left) plots of CS in 0.5 mol L⁻¹ HCl, in the absence and presence of varying dosages of the DDIP compound. The impedance spectra have only one semicircle. This suggests that the dissolution of CS in 0.5 mol L⁻¹ HCl acid is associated

with the charge transfer and double-layer nature of the corrosion process.³⁴ The diameter of the capacitive loop increases with DDIP dosage. This implies that, as the inhibitor dose increases, so does the impedance of the inhibited substrate. The frequency dispersion effect may be seen because these impedance spectra are not perfectly symmetrical semicircles. This abnormal behavior is commonly attributed to the imperfections and nonuniformity of the CS surface.³⁵ As seen in Figure 4 (left), the impedance spectra of the Bode plots show only one semicircle correlating to one time constant. It is reasonable to conclude that the charge transfer resistance R_{ct} increases when inhibitor dose increases. On the other hand, the double-layer capacitance (C_{dl}) values decrease. This is mainly due to a reduction in the local dielectric constant and/or a growth in the thickness of the double layer.³⁶ The equivalent circuit shown in Figure 5 is being used to analyze the Nyquist curves, which comprises R_s and CPE (constant phase element) parallel to the R_{ct} .

**Figure 5. Equivalent circuit model used to fit experimental EIS data.****Figure 4. Nyquist (right) and Bode (left) plots for the corrosion of CS in 0.5 mol L⁻¹ HCl without and with different concentrations of the DDIP compound at 25 °C.**

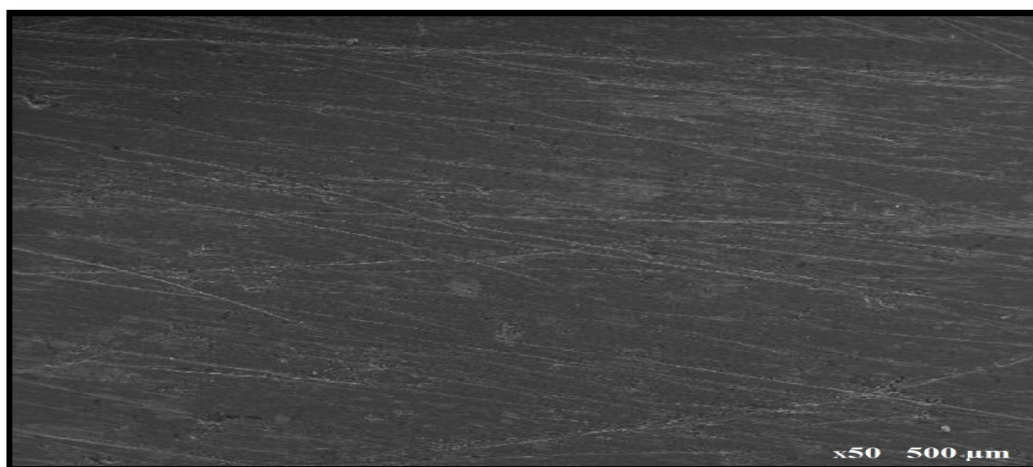


Figure 6. Pure CS after polishing.

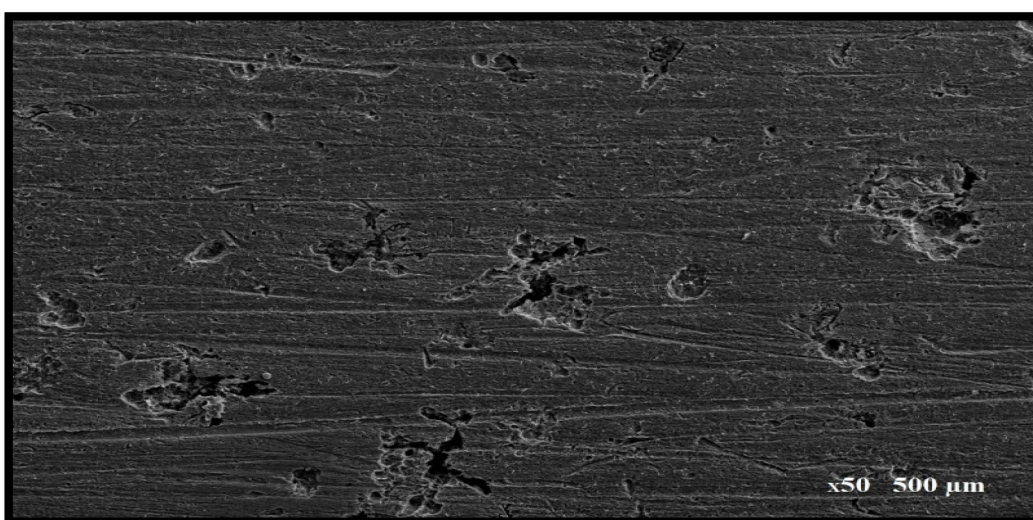


Figure 7. CS after being immersed in 0.5 mol L⁻¹ HCl.

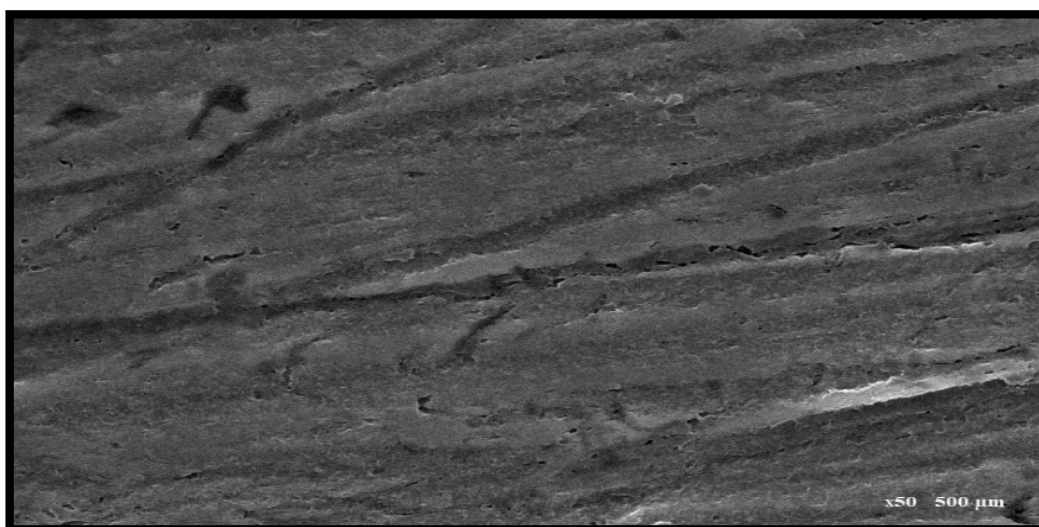


Figure 8. CS after being immersed in 0.5 mol L⁻¹ HCl + 300 ppm DDIP.

It can be observed that the magnitudes of mitigating efficiency estimated by PP and EIS methodologies differ just a

little. The discrepancy between the values was attributed to variations in the surface state of the electrode material.³⁷

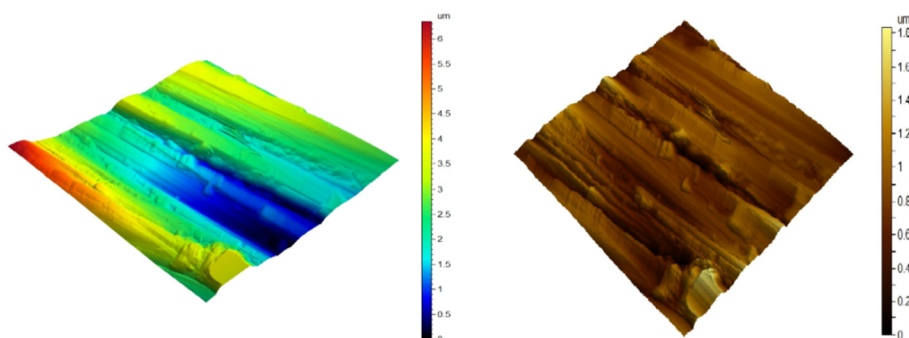


Figure 9. AFM three-dimensional picture of pure CS.

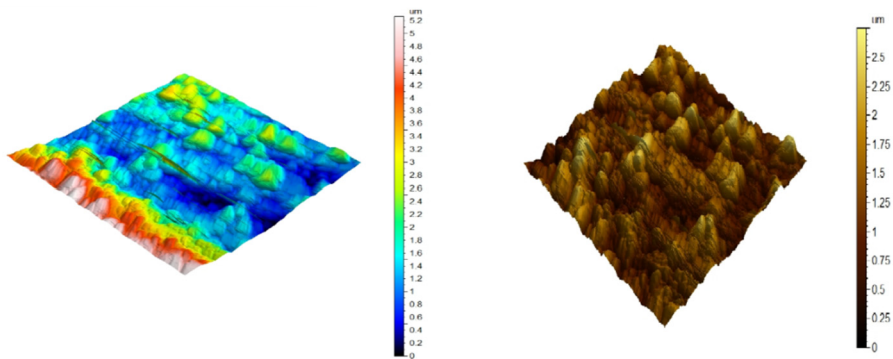


Figure 10. AFM three-dimensional picture of CS surface after being immersed for 48 h in 0.5 mol L⁻¹ HCl.

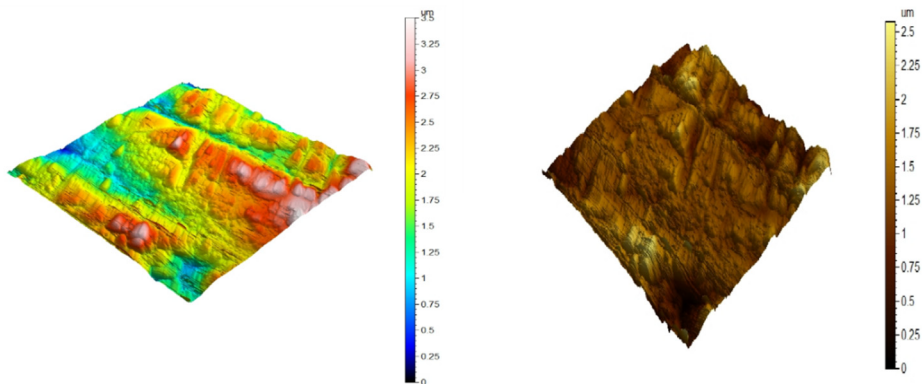


Figure 11. AFM three-dimensional picture of CS after being immersed for 48 h in 0.5 mol L⁻¹ HCl + 300 ppm DDIP.

3.7. Surface Studies. **3.7.1. SEM Investigation.** Figure 6 shows SEM image of the polished surface of CS before immersion in the test solution (0.5 mol L⁻¹ HCl). Figures 7 and 8 show the morphology of CS specimens in the absence and presence of 300 ppm of the organic compound after 48 h of exposure in 0.5 mol L⁻¹ HCl solution at room temperature. The CS surface of the blank specimen suffers greatly from pitting corrosion (Figure 7). However, in the presence of the DDIP compound, the surface is smooth and compact (Figure 8). The surface became isolated from the corrosive medium because of the adsorption of the DDIP compound on the CS surface and the formation of a protective film.

3.7.2. AFM Characterization. AFM is utilized to test the surface appearance at the pico- to microscales. It is a stunning and innovative tool for examining the effect of the inhibitor on the corrosion process at the CS solution boundary. Figures 9–11) illustrate the three-dimensional (3D) AFM morphol-

ogies of CS in 0.5 mol L⁻¹ HCl in the presence and absence of the optimum concentration (300 ppm) of the DDIP compound. The surface of the CS in 0.5 mol L⁻¹ HCl is significantly more damaged than the surface of the CS in the presence of the organic compound. In addition, the average roughness of CS in the blank solution is 0.254 μm . In the presence of the DDIP compound, the mean roughness is reduced to 0.155 μm . This implies that the organic compound is adsorbed on the CS surface and constitutes a protective film that isolates the CS surface from the aggressive HCl solution. All height parameters are given in Table 8, with the arithmetic mean height (S_a), the root-mean-square height (S_q), the maximum peak height (S_p), the maximum pit height (S_v), and the maximum height (S_z) computed in micrometer units according to ISO 25178.³⁸

3.8. DFT Results. DFT simulations were utilized to investigate the interaction type between the DDIP compound's

Table 8. AFM Parameters of CS

substance	S_a (μm)	S_q (μm)	S_p (μm)	S_v (μm)	S_z (μm)
control	0.045	0.062	0.234	0.436	0.670
0.5 mol L ⁻¹ HCl	0.254	0.351	6.040	3.560	9.600
DDIP	0.155	0.208	0.855	1.510	2.370

adsorption centers and the CS surface. The highest occupied molecular orbitals (HOMOs) and the lowest unoccupied molecular orbitals (LUMOs) for the optimized structure are presented in Figure 12. The energy gap (ΔE) between E_{HOMO} and E_{LUMO} is computed. Other variables that influence the nature of the interaction between the DDIP molecule and the CS, such as ionization potential (I), electron affinity (A), electronegativity (χ), chemical potential (μ), hardness (η), softness (σ), electrophilicity (ω), total negative charge (TNC), and total energy (E_t) were estimated by the subsequent relationships³⁹ and are listed in Table 9.

$$\Delta E = E_{\text{LUMO}} - E_{\text{HOMO}} \quad (7)$$

$$I = -E_{\text{HOMO}} \quad (8)$$

$$A = -E_{\text{LUMO}} \quad (9)$$

$$\mu = -\chi \quad (10)$$

$$\mu = \frac{(E_{\text{HOMO}} + E_{\text{LUMO}})}{2} \quad (11)$$

$$\eta = \frac{(E_{\text{LUMO}} - E_{\text{HOMO}})}{2} \quad (12)$$

$$\sigma = 1/\eta \quad (13)$$

Quantum mechanics computations were used to assess the effect of structural parameters on inhibitor efficacy and to investigate the mechanism of adsorption at the CS surface. The DDIP's molecular and electronic characteristics were determined by optimizing the lengths and angles of its bonds and the distortion angles. Figure 12 depicts the estimated configurations with the lowest energy gained from these calculations. As a result of the electron sharing between the oxygen in the DDIP and the CS, the studied inhibitor may adsorb at the CS surface.⁴⁰ The computations revealed that the geometrical structures of the examined organic compound are virtually planar, as illustrated in Figure 12. The chemical

reactivity is determined by the interaction of HOMO and LUMO levels.⁴¹

E_{HOMO} denotes the molecule's ability to give electrons to a convenient acceptor with vacant molecular orbitals, whereas E_{LUMO} denotes its ability to gain electrons. The smaller the value of E_{LUMO} , the greater the molecule's capability to receive electrons.⁴² The larger the inhibitor's E_{HOMO} value, the easier it is to supply electrons to the vacant d-orbital of the CS and the better the inhibiting efficacy. The DFT results revealed that the organic inhibitor had a high E_{HOMO} of -0.250 au, as shown in Table 9. This could explain why the DDIP inhibitor has a great potential to adsorb on the CS surface.

The structure was discussed and rationalized using the dipole moment, D .⁴³ D is the energy's first derivative. Table 9 shows a strong correlation between D and inhibition efficiency. Another quantum parameter derived from the computations is the molecule volume. The progressive increase in inhibitor molecular volume indicates that the metal surface area covered/protected by the inhibitor molecules is gradually enhanced by extending the length of the hydrophobic chain. This observation is consistent with the findings of the polarization and impedance experiments. The inhibitor DDIP has a large molecular volume of 134.66 cm³ mol⁻¹. This improves the inhibitor's inhibition efficacy by expanding the surface contact between the inhibitor's molecules and the metal surface. This is consistent with the experimental findings. The η and σ are essential qualities that assess a molecule's stability and reactivity, and they agree with experimental evidence. Furthermore, the calculations revealed that the DDIP inhibitor has a low χ and ω and a high TNC ($-5.667e$) (Table 9), which increases its donating capability to the CS surface and, as a result, its inhibitory efficacy.

The preceding section concludes that the quantum characteristics confirm that the DDIP compound has high inhibition efficiency, according to the experimental findings. In addition, the HOMO level of the inhibitor is mainly localized at the lone pairs of oxygen atoms in the OCH₃ moiety and as the π -bonding character of the C–C bond of the phenyl moiety. This indicates that these moieties are the favorite centers for the electrophilic attack on the CS surface, as shown in Figure 12. This also implies that the phenyl moiety, which has a high coefficient of HOMO density, was orientated toward the CS surface, and that adsorption happens most likely via its π -electrons.

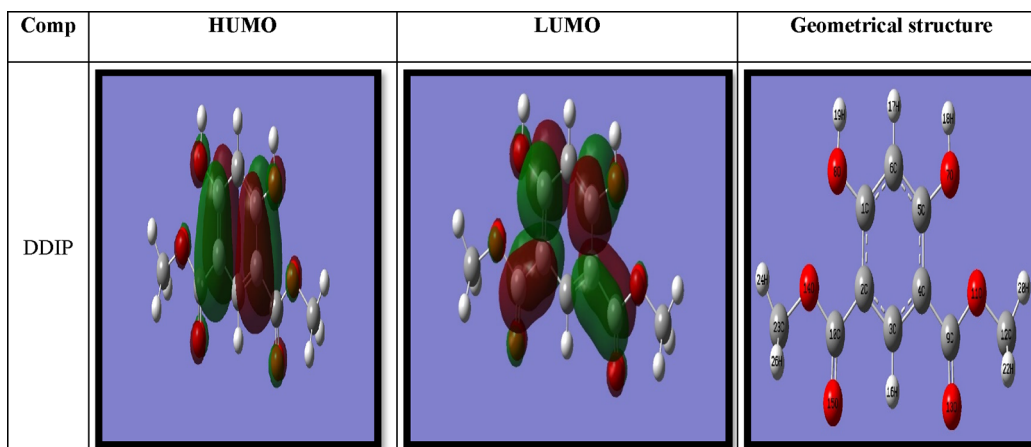
**Figure 12.** Geometrical structure and charge density distribution of HOMO and LUMO levels of the inhibitor compound DDIP.

Table 9. Calculated Quantum Chemical Parameters Obtained from DFT Theory

HOMO (au)	LUMO (au)	ΔE (au)	D (Debye)	η (au)	σ (au)	μ (au)	χ (au)	ω (au)	TNC	total energy (E_t)	volume (cm^3/mol)
-0.250	-0.053	0.197	7.178	0.099	10.101	-0.152	0.152	0.117	-5.667	-838.45	134.66

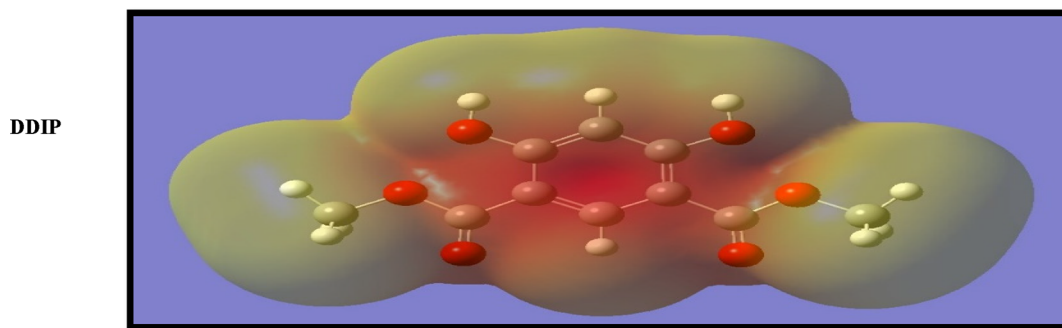


Figure 13. Electron density plots of molecular electrostatic potentials of the DDIP inhibitor.

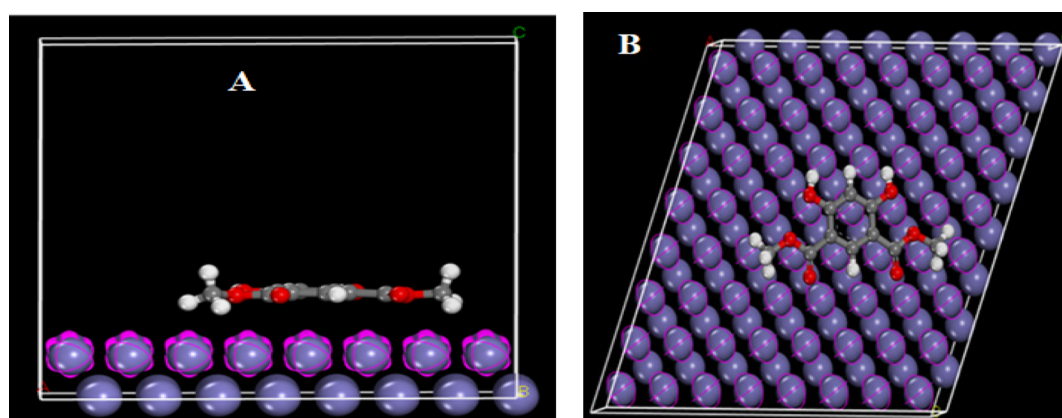


Figure 14. Side view (A) and top view (B) for the adsorption of the DDIP inhibitor on CS.

Moreover, the calculations revealed that the charge density of the LUMO level is localized as the antibonding character of the C–C phenyl moiety and C=O groups for the examined compound, implying that these moieties might be reacted as an electrophile, as shown in Figure 13. Molecular electrostatic potentials are immensely beneficial in that negative regions could be viewed as nucleophile sites, while positive electrostatic potential regions can be considered potential electrophile sites. In addition, the electrostatic potential reveals the polarization of the electron density. The results revealed that the oxygen atom has a negative electrostatic potential, implying that these centers are energetically favorable for attachment to the metal surface (Figure 13). According to the results obtained, the quantum chemical calculations demonstrate a strong link between the examined inhibitor's quantum chemical characteristics and its experimental inhibition efficacy for CS corrosion.

3.9. Monte Carlo Simulation. Monte Carlo simulation is a molecular mechanics-based simulation in which simulated annealing is used as an optimization method.⁴⁴ The advantage of MC simulation over quantum mechanical simulation is that it is much less time-consuming and hence causes cost reduction. The type of adsorption is determined by the inhibitor's molecular structure. The MC simulations were used to investigate the steel surface's adsorption behavior and the mechanism of interactions between the inhibitor molecule and the metal surface. The side and top views of the adsorption

modeling of the studied inhibitor on the surface of CS are shown in Figure 14. The following equation was used to calculate the interaction energy (binding energy) between the examined molecule and the CS surface:

$$E_{\text{ads}} = E_{\text{Fe-inh}} - (E_{\text{inh}} - E_{\text{Fe}}) \quad (14)$$

where E_{inh} and E_{Fe} are the total energy of the inhibitor and the total energy of the Fe surface, respectively. The data obtained from MC simulation (Table 10) show that the DDIP inhibitor's binding energy and Fe surface is $-528.38 \text{ kJ mol}^{-1}$. These findings corroborate the findings of the experiments.

4. CONCLUSIONS

A resorcinol derivative, DDIP, is examined as a corrosion inhibitor for low CS in 0.5 mol L^{-1} HCl acid. The mitigation efficacy increases from 61.8 to 79.9% as the DDIP dose increases from 50 to 300 ppm. However, inhibition efficiency

Table 10. Descriptors Calculated by the Monte Carlo Simulation for Adsorption of the Inhibitor on the CS Surface

molecule	total energy (kJ mol^{-1})	adsorption energy (kJ mol^{-1})	deformation energy (kJ mol^{-1})	rigid adsorption energy (kJ mol^{-1})
DDIP	-43.93	-528.38	-33.35	-495.15

decreases to 70.05% as the temperature reaches 55 °C. The compound's inhibition is due to creating a protective film at the CS. Polarization findings showed that the compound functions as a mixed-type inhibitor. The DDIP compound's adsorption obeys the Langmuir model. The results gathered through multiple methodologies were closely connected, indicating validity and correctness. The lower energy gap between the HUMO and LUMO leads to a more substantial contact between the DDIP molecule and the CS via electron donation and acceptance. The molecular dynamic simulation confirmed that the nature of the adsorption depends on the molecular structure of the inhibitor. The binding energy for the DDIP inhibitor and Fe surface is $-528.38 \text{ kJ mol}^{-1}$. The quantum characteristics confirmed that the inhibitor has high inhibition efficiency, which is consistent with the findings of the experimental results. SEM and AFM revealed the development of a uniform layer at CS in the presence of the DDIP.

■ ASSOCIATED CONTENT

SI Supporting Information

The Supporting Information is available free of charge at <https://pubs.acs.org/doi/10.1021/acsomega.2c00153>.

The ^1H NMR and ^{13}C NMR spectra (PDF)

■ AUTHOR INFORMATION

Corresponding Author

Mostafa A. A. Mahmoud – Department of Chemistry, Faculty of Science, Suez Canal University, Ismailia 41522, Egypt;
orcid.org/0000-0001-6229-3484;
Phone: +201063644726; Email: maam403.ms@gmail.com

Authors

Medhat M. Kamel – Department of Chemistry, Faculty of Science, Suez Canal University, Ismailia 41522, Egypt
Salah M. Rashwan – Department of Chemistry, Faculty of Science, Suez Canal University, Ismailia 41522, Egypt
Sameh A. A. El-Mekawy – Department of Physics and Mathematics, Faculty of Engineering, Port Said University, Port Said 41522, Egypt
Mohamed K. Awad – Theoretical Applied Chemistry Unit (TACU), Chemistry Department, Faculty of Science, Tanta University, Tanta 44213, Egypt
Hoyeda E. Ibrahim – Department of Chemistry, Faculty of Science, Suez Canal University, Ismailia 41522, Egypt

Complete contact information is available at:
<https://pubs.acs.org/doi/10.1021/acsomega.2c00153>

Notes

The authors declare no competing financial interest.

■ ACKNOWLEDGMENTS

We do acknowledge for General Petroleum Company for providing lab facilities for this work.

■ REFERENCES

- (1) Abbasov, V. M.; Abd El-Lateef, H. M.; Aliyeva, L. I.; Qasimov, E. E.; Ismayilov, I. T.; Khalaf, M. M. A study of the corrosion inhibition of mild steel C1018 in CO_2 -saturated brine using some novel surfactants based on corn oil. *Egypt. J. Pet.* **2013**, *22*, 451–470.
- (2) Olasunkanmi, L. O.; Sebona, M. F.; Ebenso, E. E. Influence of 6-phenyl-3 (2H)-pyridazinone and 3-chloro-6-phenylpyrazine on mild steel corrosion in 0.5 M HCl medium: experimental and theoretical studies. *J. Mol. Struct.* **2017**, *1149*, 549–559.
- (3) Migahed, M.A.; EL-Rabiei, M. M.; Nady, H.; Elgendy, A.; Zaki, E.G.; Abdou, M.I.; Noamy, E. S. Novel Ionic Liquid Compound Act as Sweet Corrosion Inhibitors for X-65 Carbon Tubing Steel: Experimental and Theoretical Studies. *J. Bio. Tribo-Corros.* **2017**, *3*, 31.
- (4) Seter, M.; Thomson, M. J.; Stoimenovski, J.; MacFarlane, D. R.; Forsyth, M. Dual active ionic liquids and organic salts for inhibition of microbially influenced corrosion. *Chem. Commun.* **2012**, *48*, 5983.
- (5) Pandey, A.; Verma, C.; Singh, B.; Ebenso, E. E. Synthesis, characterization and corrosion inhibition properties of benzamide-2-chloro-4-nitrobenzoic acid and anthranilic acid-2-chloro-4-nitrobenzoic acid for mild steel corrosion in acidic medium. *J. Mol. Struct.* **2018**, *1155*, 110–122.
- (6) Popoola, L. T.; Grema, A. S.; Latinwo, G. K.; Gutti, B.; Balogun, A. S. Corrosion problems during oil and gas production and its mitigation. *Int. J. Ind. Chem.* **2013**, *4*, 35.
- (7) Subramania, A.; Kalyana Sundaram, N. T.; Sathiya Priya, R.; Saminathan, K.; Muralidharan, V. S.; Vasudevan, T. Aldimines, Aldimines – effective corrosion inhibitors for mild steel in hydrochloric acid solution. *J. Appl. Electrochem.* **2004**, *34*, 693–696.
- (8) Migahed, M. A.; EL-Rabiei, M. M.; Nady, H.; Elgendy, A.; Zaki, E. G.; Abdou, M. I.; Noamy, E. S. Novel Ionic Liquid Compound Act as Sweet Corrosion Inhibitors for X-65 Carbon Tubing Steel: Experimental and Theoretical Studies. *J. Bio. Tribo-Corros.* **2017**, *3*, 31.
- (9) Hasan, B. O.; Sadek, S. A. The effect of temperature and hydrodynamics on carbon steel corrosion and its inhibition in oxygenated acid-salt solution. *J. Ind. Eng. Chem.* **2014**, *20*, 297–307.
- (10) Migahed, M. A.; Al-Sabagh, A. M.; Zaki, E. G.; Mostafa, H. A.; Fouda, A. S. Synthesis of Some Novel Cationic Surfactants and Evaluation of Their Performance as Corrosion Inhibitors for X-65 type Carbon Steel under H_2S Environment. *Int. J. Electrochem. Sci.* **2014**, *9*, 7693–7711.
- (11) Ahamad, I.; Prasad, R.; Quraishi, M.A. Experimental and theoretical investigations of adsorption of fexofenadine at mild steel/hydrochloric acid interface as corrosion inhibitor. *J. Solid State Electrochem* **2010**, *52*, 933–942.
- (12) Yurt, A.; Aykin, O. Diphenolic Schiff bases as corrosion inhibitors for aluminium in 0.1 M HCl: Potentiodynamic polarisation and EQCM investigations. *Corros. Sci.* **2011**, *53*, 3725–3732.
- (13) Chetouani, A.; Hammouti, B.; Benhadda, T.; Baoudi, M. Inhibitive action of bipyrazolic type organic compounds towards corrosion of pure iron in acidic media. *Appl. Surf. Sci.* **2005**, *249*, 375–385.
- (14) Quraishi, M. A.; Sardar, R. Aromatic Triazoles as Corrosion Inhibitors for Mild Steel in Acidic Environments. *Corrosion* **2002**, *58*, 748–755.
- (15) Juttner, K. Electrochemical impedance spectroscopy (EIS) of corrosion processes on inhomogeneous surfaces. *Electrochim. Acta* **1990**, *35*, 1501–1508.
- (16) Nathiya, R. S.; Perumal, S.; Moorthy, M.; Murugesan, V.; Rangappan, R.; Raj, V. Synthesis, Characterization and Inhibition Performance of Schiff Bases for Aluminium Corrosion in 1 M H_2SO_4 Solution. *J. Bio Tribo Corros.* **2020**, *6*, 5.
- (17) Chen, S.; Zhu, B.; Liang, X. Corrosion Inhibition Performance of Coconut Leaf Extract as a Green Corrosion Inhibitor for X65 Steel in Hydrochloric Acid Solution. *Int. J. Electrochem. Sci.* **2020**, *15*, 1–15.
- (18) Fouda, A. S.; Rashwan, S. M.; Kamel, M. M.; Haleem, E. A. Chemical, electrochemical and surface morphology investigation of Cichorium intybus extract (CIE) as beneficial inhibitor for Al in 2 M HCl acid. *Lett. Appl. NanoBioScience* **2021**, *9* (2), 1064–1073.
- (19) Fouda, A. S.; Rashwan, S. M.; Kamel, M. M.; Haleem, E. A. Juglans Regia Extract (JRE) as Eco-Friendly Inhibitor for Aluminum Metal in Hydrochloric Acid Medium. *Biointerface Res. Appl. Chem.* **2020**, *10* (5), 6398–6416.

- (20) Kamel, M.; Hegazy, M.; Rashwan, S.; El Kotb, M. Innovative surfactant of Gemini-type for dissolution mitigation of steel in pickling HCl medium. *Chin. J. Chem. Eng.* **2021**, *34*, 125–133.
- (21) Nafie, M. S.; Arafa, K.; Sedky, N. K.; Alakhdar, A. A.; Arafa, R. K. Triaryl Dicationic DNA Minor-Groove Binders with Antioxidant Activity Display Cytotoxicity and Induce Apoptosis in Breast Cancer. *Chemico-Biological Interactions* **2020**, *324*, 109087.
- (22) Nafie, M. S.; Amer, A. M.; Mohamed, A. K.; Tantawy, E. S. Discovery of Novel Pyrazolo[3,4-b]Pyridine Scaffold-Based Derivatives as Potential PIM-1 Kinase Inhibitors in Breast Cancer MCF-7 Cells. *Bioorg. Med. Chem.* **2020**, *28* (24), 115828.
- (23) Kamel, M. M.; Mohsen, Q.; Anwar, Z. M.; Sherif, M. A. An expired ceftazidime antibiotic as an inhibitor for disintegration of copper metal in pickling HCl media. *J. Mater. Res. Technol.* **2021**, *11*, 875–886.
- (24) Zeng, H.; Miller, R. S.; Flowers, R. A.; Gong, B. A Highly Stable, Six-Hydrogen-Bonded Molecular Duplex. *J. Am. Chem. Soc.* **2000**, *122*, 2635–2644.
- (25) Stern, M.; Geaby, A. L. Electrochemical Polarization: I. A Theoretical Analysis of the Shape of Polarization Curves. *J. Electrochem. Soc.* **1957**, *104* (1), 56–63.
- (26) Perez, N. *Electrochemistry and corrosion science* **2016**, 1–23.
- (27) Elachouri, M.; Hajji, M. S.; Salem, M.; Kertit, S.; Aride, J.; Coudert, R.; Essassi, E. Some Nonionic Surfactants as Inhibitors of the Corrosion of Iron in Acid Chloride Solutions. *Corrosion* **1996**, *52*, 103.
- (28) Bentiss, F.; Lebrini, M.; Lagrenée, M. Thermodynamic characterization of metal dissolution and inhibitor adsorption processes in mild steel/ 2,5-bis(n-thienyl)-1,3,4-thiadiazoles/ hydrochloric acid system. *Corros. Sci.* **2005**, *47*, 2915–2931.
- (29) Langmuir, I. The constitution and fundamental properties of solids and liquids. *J. Am. Chem. Soc.* **1916**, *38*, 2221–2295.
- (30) Schorr, M.; Yahalom, J. The significance of the energy of activation for the dissolution reaction of metal in acids. *Corros. Sci.* **1972**, *12* (11), 867–868.
- (31) Ekanem, U. F.; Umoren, S. A. Inhibition of mild steel corrosion in h2so4 using exudate gum from pachylobus edulis and synergistic potassium halide additives. *Chem. Eng. Commun.* **2010**, *197*, 1339–1356.
- (32) Latour, R. A. The langmuir isotherm: A commonly applied but misleading approach for the analysis of protein adsorption behavior. *J. Biomed. Mater. Res., Part A* **2015**, *103* (3), 949–958.
- (33) Gopi, D.; Govindaraju, K. M.; Kavitha, L. Investigation of triazole derived Schiff bases as corrosion inhibitors for mild steel in hydrochloric acid medium. *J. Appl. Electrochem.* **2010**, *40*, 1349–1356.
- (34) Essaghouani, A. L.; Elmsellem, H.; Boulhaoua, M.; Ellouz, M.; El Hafi, M.; Sebbar, N. K.; Essassi, E. M.; Bouabdellaoui, M.; Aouniti, A.; Hammouti, B. Adsorption proprieties and inhibition of mild steel corrosion in HCl solution by 1-Benzyl-4-phenyl-2,3-dihydro-1H-1,5-benzodiazepin-2-one. *Der Pharma Chemica.* **2016**, *8* (2), 347–355.
- (35) Singh, A. K.; Quraishi, M. A. Investigation of the Effect of Disulfiram on Corrosion of Mild Steel in Hydrochloric Acid Solution. *Corros. Sci.* **2011**, *53*, 1288–1297.
- (36) Issaadi, T.; Douadi, A.; Zouaoui, S.; Chafaa, M.; Khan, A.; Bouet, G. Novel thiophene symmetrical Schiff base compounds as corrosion inhibitor for mild steel in acidic media. *Corros. Sci.* **2011**, *53*, 1484–1488.
- (37) Kamel, M. M.; Fouda, A. S.; Rashwan, S. M.; Abdelkader, O. Paprika extract: a green inhibitor for mitigating carbon steel disintegration in 1 M HCl pickling solution. *Green Chem. Lett. Rev.* **2021**, *14* (4), 600–611.
- (38) Introduction to Surface Roughness Measurement, International Organization for Standardization ISO 25178; https://sernia.ru/upload/pdf_files/Introduction%20to%20surface%20roughness%20measurement.pdf (accessed 2022-04-19).
- (39) Hegazy, M. A.; Rashwan, S. M.; Meleek, S.; Kamel, M. M. Synthesis, characterization and mitigation action of innovative Schiff base on steel disintegration in sulfuric acid solution. *Mater. Chem. Phys.* **2021**, *267* (5), 124697.
- (40) Lalitha, A.; Ramesh, S.; Rajeswari, S. Surface protection of copper in acid medium by azoles and surfactants. *Electrochim. Acta* **2005**, *51*, 47.
- (41) Zhang, D. Q.; Gao, L. W.; Zhou, G. D. Inhibition of copper corrosion in aerated hydrochloric acid solution by heterocyclic compounds containing a mercapto group. *Corros. Sci.* **2004**, *46*, 3031.
- (42) Negm, N. A.; Migahed, M. A.; Farag, R. K.; Fadda, A. A.; Awad, M. K.; Shaban, M. M. High performance corrosion inhibition of novel tricationic surfactants on carbon steel in formation water: Electrochemical and computational evaluations. *J. Mol. Liq.* **2018**, *262*, 363.
- (43) Martinez, S. Inhibitory mechanism of mimosa tannin using molecular modeling and substitutional adsorption isotherms. *Mater. Chem. Phys.* **2003**, *77*, 97–102.
- (44) Kirkpatrick, S.; Gelatt, C. D.; Vecchi, M. P. Optimization by Simulated Annealing. *Science* **1983**, *220*, 671–680.